# Coacervate of a Commercial Non-Sulfate Shampoo: Preliminary Studies of Their Structure via Turbidity, Dynamic Light Scattering, ζ-Potential, Fluorescence, Rheology, Small-Angle X-Ray Scattering and Microscopy Measurements

Hikari Kamo<sup>1</sup>, Toshihiro Mori<sup>1,2</sup> and Katsunori Yoshida\*,<sup>1</sup>

<sup>1</sup>Skin Science Lab, School of Pharmacy, Kitasato University, Tokyo, Japan

<sup>2</sup>Skincare Lab, Mandom Corporation, Osaka, Japan

Shampoos are commonly formulated with cationic polymers, anionic surfactants, and amphoteric surfactants. When diluted with water, these components can undergo liquid-liquid phase separation, or coacervation, at specific relative concentrations. Traditionally, shampoos have used sulfate-based surfactants such as sodium lauryl sulfate (LS) and lauryl ether sulfate (LES). However, due to increasing concerns about skin sensitivity and environmental impact, non-sulfate surfactants, such as those derived from amino acids, have become more popular. Despite this shift in formulation, studies on coacervates formed by non-sulfate shampoos are relatively scarce. In this study, we focused on examining the coacervates that form during the dilution process of a commercially available non-sulfate shampoo. We employed a variety of analytical techniques, including turbidity measurements, dynamic light scattering, ζ-potential analysis, rheology, small-angle X-ray scattering (SAXS), and microscopy, to investigate the structural changes of these coacervates throughout the dilution process. Our findings revealed that as the shampoo is diluted, the coacervates exhibit increased elasticity, and at specific relative concentrations, they form a lamellar structure. Additionally, we observed significant structural transitions as dilution progressed further. These results contribute to a deeper understanding of coacervation in non-sulfate shampoos and provide insight into the structural characteristics that differentiate them from traditional sulfate-based shampoos. Further investigation of a model formulation with a well-defined composition is needed to explore the broader implications of these findings on shampoo formulation and performance.

Key words: coacervate, shampoo, non-sulfate, dilution, mixed micelle, anionic surfactant, amphoteric surfactant, polycation, structural change, lamellar phase, turbidity, dynamic light scattering (DLS),  $\zeta$ -potential, fluorescence, rheology, small-angle X-ray scattering (SAXS), polarized light microscopy, transmission electron microscopy (TEM)

Received: December 18, 2024; Accepted: May 13, 2025

\*Corresponding author: Katsunori Yoshida (E-mail: yoshida.katsunori@kitasato-u.ac.jp)

Skin Science Lab, School of Pharmacy, Kitasato University, 5-9-1, Shirokane, Minato-ku, Tokyo 108-8641, Japan

DOI: 10.69336/acst.2024-14



 $\ensuremath{\mathbb{C}}$  The Society of Cosmetic Chemists of Japan 2025

This article is licensed under a Creative Commons Attribution 4.0 International License.

# 1. Introduction

Surfactant micelles and oppositely charged polyelectrolytes undergo strong electrostatic interactions in aqueous solutions, leading to either solid–liquid or liquid–liquid phase separation. The latter process is known as coacervation, where a concentrated phase (coacervate) and a dilute phase are formed.<sup>1–15)</sup> The coacervate has found applications in various fields, including personal care, food products, water treatment, drug delivery (e.g., for water-soluble anticancer drugs), and DNA transfection.<sup>2,3,16–23)</sup> Coacervation occurs only under specific conditions and is driven by the interaction of multiple factors. These factors include polymer properties (polymer charge density, molecular weight, concentration, and molecular structure), micellar properties (surface charge density, surfactant mixing molar ratio, size, and concentration), temperature, and ionic strength.<sup>4–6,24–32)</sup>

Dubin et al. reported that the formation of soluble complexes, which are precursors to coacervates, plays a key role in controlling coacervation.<sup>1,4,5)</sup> Ilekti et al. studied coacervation in detail by diluting a system composed of sodium polyacrylate (NaPA) and cetyltrimethylammonium bromide (CTABr) with water.<sup>33,34)</sup> They observed that water addition induced the separation of the system into a concentrated phase and a dilute phase, with further water addition concentrating the coacervate. During this process, Br<sup>-</sup> ions bound to surfactant molecules were replaced by PA<sup>-</sup> ions through an ion-exchange mechanism. This ion exchange led to the migration of simple ions such as Br<sup>-</sup> and Na<sup>+</sup> to the dilute phase, increasing the overall entropy of the system and driving the coacervation process.

Common shampoo formulations include cationic polymers as conditioning agents and anionic and amphoteric surfactants as detergents. When diluted with water during use, these ingredients undergo phase separation, forming coacervates—water-insoluble substances. The properties of the coacervates are known to influence the sensory experience of the shampoo. <sup>2,3,30,35,36)</sup> In formulation development, this sensory aspect is often empirically adjusted by altering the type, quantity, and combination of cationic polymers and surfactants. Ghasemi et al. developed a molecular thermodynamic model to predict the formation and phase behavior of coacervates in systems containing cationic polymers and anionic surfactants. <sup>16)</sup> This model has been shown to accurately predict coacervate properties under various conditions. As the relationship between coacervate properties and the sensory characteristics of shampoos becomes better understood, shampoo formulation development is advancing from an empirical approach to a more systematic one, offering valuable insights for optimizing shampoo formulations.

In recent years, driven by the Sustainable Development Goals and an increasing preference for natural ingredients, the use of non-sulfate surfactants such as amino acid-based surfactants in shampoo formulations has become more wide-spread. Compared to traditional lauryl sulfate (LS) and lauryl ether sulfate (LES) shampoos, non-sulfate alternatives face challenges such as poor foaming and thickening. However, due to their high biodegradability and lower potential for skin irritation, they have become the dominant products in the market. While significant knowledge has been accumulated regarding the coacervates formed by LS/LES surfactant shampoos, the properties of coacervates formed by non-sulfate shampoos, which represent a newer trend, have not been thoroughly documented. We previously reported a study investigating the relationship between coacervate properties and the sensory attributes of non-sulfate commercial shampoos. The findings revealed that even in non-sulfate shampoos, the properties of the coacervates significantly influenced the sensory experience. In this study, we focus on the structural changes in the coacervates formed by a non-sulfate commercial shampoo during dilution with water.

# 2. Materials and Methods

## 2.1. Materials

A commercially available non-sulfate shampoo, purchased at a drugstore in Tokyo in March 2024, was used for this study. Table 1 shows the complete ingredient list of the shampoo provided on the product label, with the order of ingredients preserved. High-purity pyrene (>99.0%), obtained from Sigma-Aldrich (St. Louis, MO, USA), was employed as a fluorescent probe without further purification. Milli-Q water (Merck Millipore, St. Louis, MO, USA), was used throughout this study.

# 2.2. Turbidity measurement in the shampoo dilution process

A fixed amount of shampoo solution was weighed and diluted with purified water under continuous stirring. The transmittance (%) of each diluted solution at 420 nm was measured using a U-2800 spectrophotometer (Hitachi, Tokyo, Japan). Turbidity was expressed as 100 – transmittance (%). The relative concentrations of diluted shampoo were calculated as follows:

Relative concentration = undiluted shampoo solution (g)/(undiluted shampoo solution (g) + added purified water (g)).

Unless otherwise specified, all measurements, including turbidity assessments, were conducted at room temperature  $(23^{\circ}\text{C} \pm 2^{\circ}\text{C})$ .

## Table 1 Ingredient list of the tested shampoo.

Water, cocamide methyl MEA, lauramidopropyl betaine, disodium laureth sulfosuccinate, isopentyldiol, sodium lauryl glycol carboxylate, sodium lauroyl aspartate, glycerin, levulinic acid, polyquaternium-10, alcohol, PEG-2 laurate, diisostearyl malate, polyquaternium-7, polyquaternium-67, meadowfoam delta-lactone, tocopherol, phenoxyethanol, fragrance

# 2.3. Coacervate formation

The shampoo and purified water were weighed into a 50-mL centrifuge tube to achieve relative concentrations between 0.02 and 0.35. After thorough mixing, the samples were centrifuged at 4400 rpm for 30 min and then left to stand overnight. The supernatant was carefully removed, and the combined weight of the coacervate and container (w, in g) was measured. The previously measured container weight ( $w_0$ , in g) was subtracted from the total (w) to determine the weight of the coacervate formed. The coacervate weight was then divided by the initial shampoo weight to calculate the amount of coacervate formed per gram of shampoo. Coacervates prepared in this manner were subsequently used to evaluate their properties.

# 2.4. Particle size and $\zeta$ -potential

The particle size and  $\zeta$ -potential of the coacervate were measured immediately after dilution using a dynamic light scattering analyzer (ELSZ-1000, Otsuka Electronics, Otsuka, Japan).  $\zeta$ -Potential measurements were repeated 3 times at each relative concentration, and the average values were calculated. Particle size, expressed as diameter, was determined using the Einstein–Stokes equation:  $D = kT/3\pi\eta d$ , where D is the mutual diffusion coefficient obtained from dynamic light scattering. The average particle size and polydispersity index (P.I.) were calculated using the cumulant method, as provided in the analysis software accompanying the measurement device.

#### 2.5. Fluorescence probe measurement

A pyrene solution was prepared at a concentration of  $0.5~\mu M$ , and the sample solutions were prepared using this solution to achieve a shampoo relative concentration range of 0.00001-0.1. Fluorescence spectra were measured using a fluorescence spectrophotometer (F-7000, Hitachi) with an excitation wavelength of 336 nm, a scanning range of 360–420 nm, an excitation slit width of 10 nm, and an emission slit width of 1 nm. The intensity ratio  $I_1/I_3$  between the first and third fluorescence peaks was then calculated.

#### 2.6. Rheological measurement

Dynamic viscoelasticity measurements were conducted on the coacervates obtained at each relative concentration, as well as on the shampoo solution. A stress-controlled rheometer (MCR-300, with a 50-mm diameter parallel plate, Anton Paar Japan, Tokyo, Japan) was used for these measurements at 25°C, with a frequency range of  $\omega = 0.1-100 \, \text{rad/s}$  and a strain amplitude of  $\gamma = 1\%$ .

#### 2.7. Polarized light microscopy

The coacervates produced at each relative concentration were observed using a polarized light microscope (OLYM-PUS BX51, equipped with sCMOS Microscope Camera Moticam S3, Shimadzu, Kyoto, Japan).

# 2.8. Transmission electron microscopy (TEM)

TEM observations were conducted at a relative concentration of 0.05 immediately after dilution of the shampoo. For TEM micrographs, 20 μL of diluted shampoo was placed on a 200-mesh poly(vinyl formal)-coated copper grid and allowed to adsorb for 1 min. Excess liquid was removed using a piece of filter paper, air-dried, and then negatively stained with 2% aqueous uranyl acetate. The specimens were further dried *in vacuo* for 5 min before use. The specimens were examined under a transmission electron microscope (JEM 1400, JEOL, Tokyo, Japan) operating at an accelerating voltage of 120 kV at room temperature.

## 2.9. Small-angle X-ray scattering (SAXS)

SAXS measurements were carried out on the coacervates obtained at each relative concentration, as well as on the shampoo solution. The measurements were performed using a SAXSpace instrument (Anton Paar) equipped with a Mythen 1K detector (Dectris, Philadelphia, PA, USA). The sample-to-detector distance was set at 317 mm, with an exposure time of 60 min. The scattered intensity profile, I(q), was obtained, where q represents the wavevector ( $q = 4\pi \sin\theta/\lambda$ ), with 2 $\theta$  as the scattering angle and  $\lambda$  as the wavelength.

## 3. Results and Discussion

#### 3.1. Turbidity measurement in the shampoo dilution process

The results of turbidity measurements during the shampoo dilution process are shown in Fig. 1. The horizontal axis represents the relative concentration of shampoo diluted with water, while the vertical axis shows turbidity. A relative

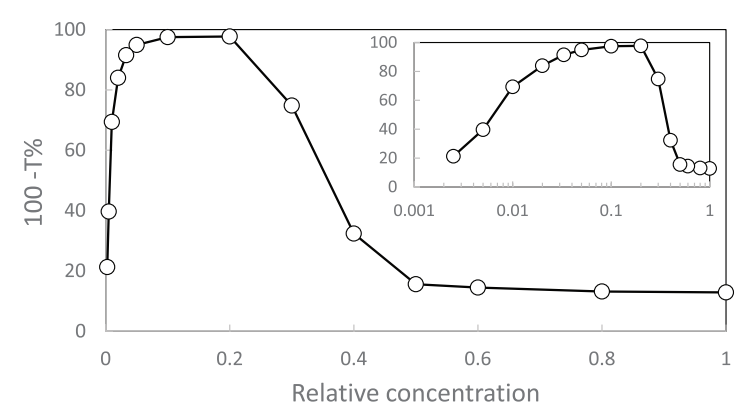


Fig. 1 Turbidity measurements of the diluted shampoo at various relative concentrations. The inset shows the same data plotted on a logarithmic scale. A relative concentration of 1 corresponds to the undiluted shampoo, which is slightly cloudy and colored, resulting in turbidity between 10% and 15% for relative concentrations ranging from 0.5 to 1.

concentration of 1, located at the right end of the horizontal axis, corresponds to the undiluted original shampoo solution, and moving leftward reflects increasing dilution, with 0.5 indicating a 2-fold dilution and 0.1 indicating a 10-fold dilution. To better visualize changes in turbidity at low relative concentrations (high dilution), the relative concentrations are displayed on a logarithmic scale in Fig. 1 (inset).

Throughout the dilution experiments, the pH remained around 6 across all relative concentrations, suggesting that the carboxyl groups of the anionic surfactants were dissociated and carried a negative charge. An increase in turbidity was observed at a relative concentration of approximately 0.4, indicating the onset of liquid–liquid phase separation phenomenon, or coacervation. As more water was added, turbidity increased sharply, peaking at relative concentrations between 0.1 and 0.2, followed by a gradual decrease in turbidity at higher dilution levels. This behavior, where turbidity rapidly rises and then gradually declines as dilution progresses, is characteristic of the bell-shaped curve typically associated with coacervation.<sup>2,5,31)</sup>

## 3.2. Coacervate formation

The amount of coacervate formed is presented in Fig. 2. At a relative concentration of 0.35, where turbidity had already begun to increase and phase separation had initiated (as shown in Fig. 1), no recoverable coacervate could be obtained by our procedure. A measurable amount of coacervate was first observed at a relative concentration of 0.3. The amount of coacervate formed increased rapidly from a relative concentration of 0.25, eventually reaching a constant value of approximately 0.2 g/1 g of shampoo solution, which was maintained down to a relative concentration of 0.02.

In a previous study conducted by the authors, which compared 4 commercially available shampoos, the amount and pattern of coacervate formation varied among the shampoos.<sup>39)</sup> The shampoo used in this study consistently produced a stable amount of coacervate, even at low relative concentrations, making it an appropriate sample for evaluating the physical properties of coacervates. No measurable coacervate was recovered at relative concentrations <0.02.

#### 3.3. Particle size and $\zeta$ -potential

Figure 3 shows the results of turbidity, particle size, and  $\zeta$ -potential measurements at each relative concentration. The particle size (d/nm) reached its maximum around a relative concentration of 0.1, coinciding with the peak in turbidity. The figure also displays the P.I. alongside the particle size, indicating that polydispersity increases as particle size increases. As the relative concentration decreases with further dilution, both particle size and the P.I. decrease in the region where turbidity also declines.

The  $\zeta$ -potential data in Fig. 3 show that while turbidity, the average particle size, and the P.I. reached a maximum at a relative concentration of 0.1 and then gradually decreased at lower relative concentrations with dilution, the  $\zeta$ -potential decreased consistently up to a relative concentration of 0.01. This suggests that the dispersion stability of the coacervate particles improved through electrostatic repulsion as dilution progressed at relative concentrations lower than 0.1. This is one of the reasons why we could not collect a measurable amount of coacervate at relative concentrations lower than 0.02 in Fig. 2. Throughout the dilution process, the  $\zeta$ -potential remained negative. The  $\zeta$ -potential values gradually decreased in negativity as dilution continued, reaching a minimum at a relative concentration of 0.01. At even lower concentrations, the  $\zeta$ -potential began to increase. It was difficult to obtain the  $\zeta$ -potential values at very low relative concentrations due to the detection limitations of the instrument.

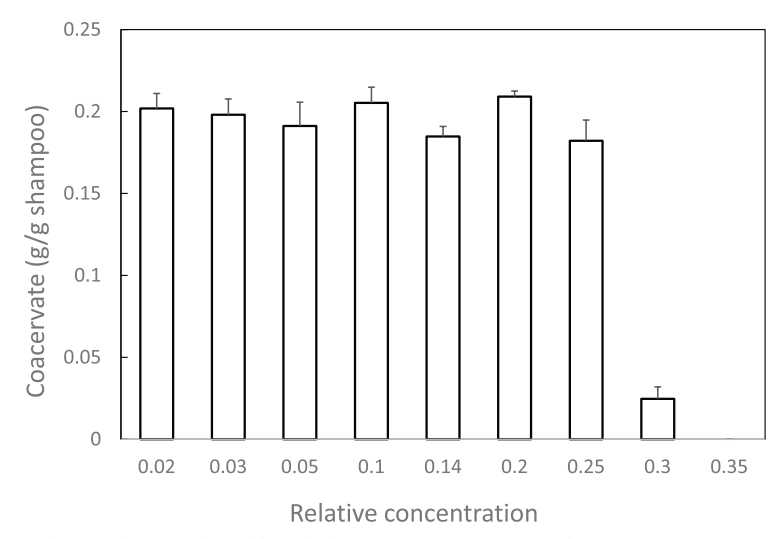


Fig. 2 Weight of coacervate formed from the diluted shampoo at various relative concentrations. No measurable coacervate was collected despite the increase in turbidity at relative concentrations  $\geq$ 0.35 and  $\leq$ 0.02, as shown in Fig. 1.

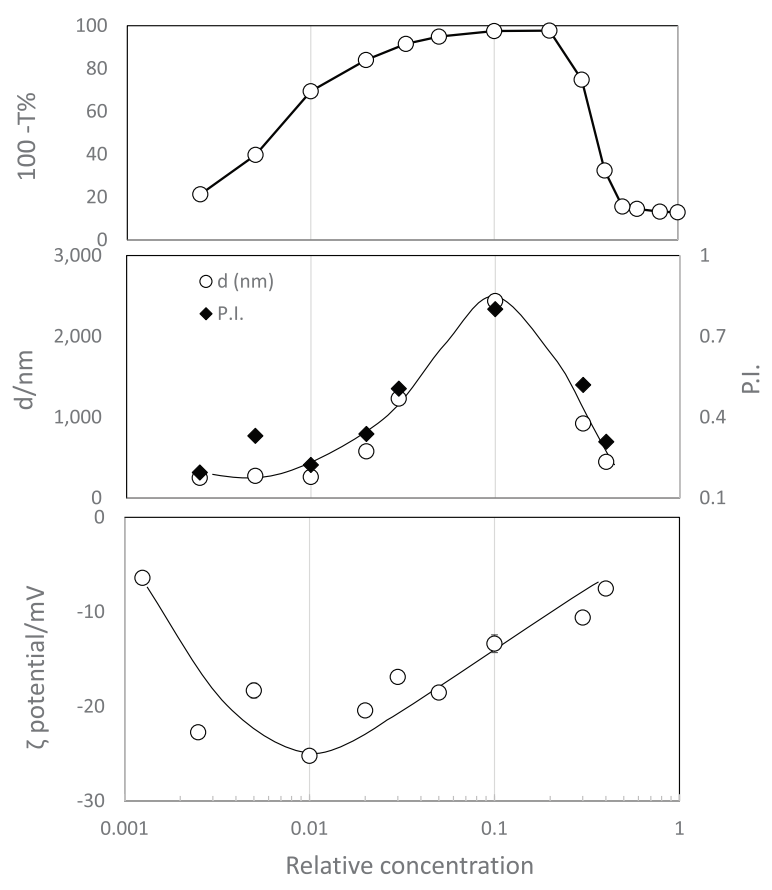


Fig. 3 Turbidity, dynamic light scattering, and ζ-potential measurements of diluted shampoo at various relative concentrations. Lines in the figures are included as visual guides. P.I., polydispersity index

Previous studies on the coacervation of polyelectrolytes and oppositely charged surfactants have reported that polymer–surfactant complexes tend to aggregate and form coacervates near electrical neutrality due to reduced electrostatic repulsion.<sup>4,5,40)</sup> Based on this, we expected the  $\zeta$ -potential to approach  $\pm 0$  mV at a relative concentration of 0.1, where turbidity and particle size both peaked. However, as shown in Fig. 3, the actual results were quite different from this expectation. We will discuss the reason in the later part of this report.

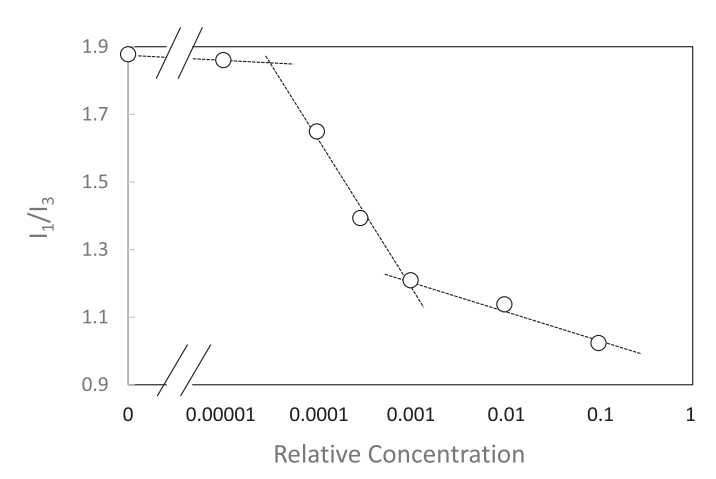


Fig. 4  $I_1/I_3$  intensity ratio for pyrene (0.5  $\mu$ M) fluorescence in diluted shampoo as a function of relative concentrations. Lines in the figure are included as visual guides.

# 3.4. Fluorescent probe measurement

To investigate the aggregation state of surfactants in highly dilute regions, we performed fluorescence measurements using pyrene as a probe. Pyrene is a fluorescent compound known to alter its fluorescence spectrum depending on the hydrophilic or hydrophobic environment in which it resides.  $^{41-43)}$  Specifically, by analyzing the ratio of the first peak of pyrene fluorescence around 374 nm ( $I_1$ ) to the third peak around 385 nm ( $I_3$ ) ( $I_1/I_3$ ), the surrounding environment of pyrene can be inferred. This method allows us to estimate the critical micelle concentration of surfactants and the critical aggregation concentration (CAC) in the presence of polymers.  $^{44}$ 

As shown in Fig. 4, the results present a typical curve with 2 inflection points, occurring around relative concentrations of 0.001 and 0.00003. In the relative concentration range above 0.001, there exists a sufficiently hydrophobic micellar core to solubilize most of the pyrene molecules in the system. However, at lower relative concentrations, the micelle concentration capable of solubilizing pyrene gradually decreases with dilution, and below a relative concentration of 0.00003, surfactant micelles are dissociated, leaving only monodisperse surfactant molecules dissolved in the system, where pyrene molecules are dissolved in water.

Considering the  $\zeta$ -potential trends discussed earlier and the fluorescence probe analysis results, it is suggested that negatively charged complexes are formed between the cationic polymers and the micelles of anionic and amphoteric surfactants upon dilution of the shampoo. While the exact charge ratio of cations to anions in the commercial shampoo is not disclosed, typical formulations are known to contain an excess molar charge ratio of anionic surfactants to cationic polymers. Compared with the previous study by Wang et al.,<sup>4,5)</sup> which was composed of an equal charge molar ratio of anions and cations, our system, consisting of an excess of anions, may cause the formation of negatively charged complexes. This hypothesis will be investigated in our next experiments using a model formulation with a well-defined composition.

Considering the mechanism of coacervation driven by entropy gain through counter-ion release,  $^{44-47)}$  dilution of shampoo with water accelerates releasing small ions (such as Na<sup>+</sup> and Cl<sup>-</sup>) into the dilute phase. This enhances the electrostatic interactions between the cationic polymer and the anionic surfactants. As dilution progresses, more anionic surfactant molecules are expected to adsorb onto the cationic polymer, increasing the number of micelles associated with the polymer. In this anion-rich system, the dilution results in a decrease in  $\zeta$ -potential as shown in Fig. 3.

At relative concentrations below 0.001, the surfactant concentration approaches the CAC, at which micelle formation diminishes. Monodisperse dissolved surfactant molecules become dominant in the system, leading to the desorption of anionic surfactants from the cationic polymer. As a result, the  $\zeta$ -potential of the polymer–surfactant complex shifts toward neutrality. Between the first and second bending points of the pyrene  $I_1/I_3$  curve (relative concentrations of 0.00003–0.001), the system may likely reach electrical neutrality. However, in this experiment, the neutralization point could not be determined as it fell below the measurable range of the instrument in such dilute regions.

#### 3.5. Rheological measurement

Figures 5 and 6 present the results of dynamic viscoelasticity measurements for both the shampoo solution and the coacervate. The  $\eta^*$  values of the coacervates show that coacervates obtained at higher dilution, corresponding to lower relative concentrations, exhibit higher viscosity, suggesting the formation of more structured viscous networks.

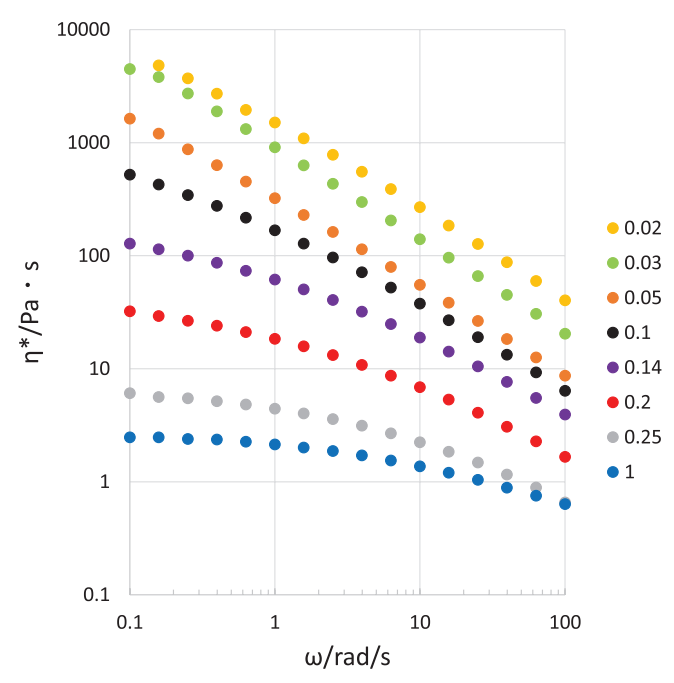


Fig. 5 Complex viscosity  $(\eta^*)$  of the coacervate formed from diluted shampoo at various relative concentrations as a function of frequency. The relative concentrations are indicated in the figure. Coacervate samples were prepared following the same procedure as described for the coacervate weight measurements in Fig. 2.

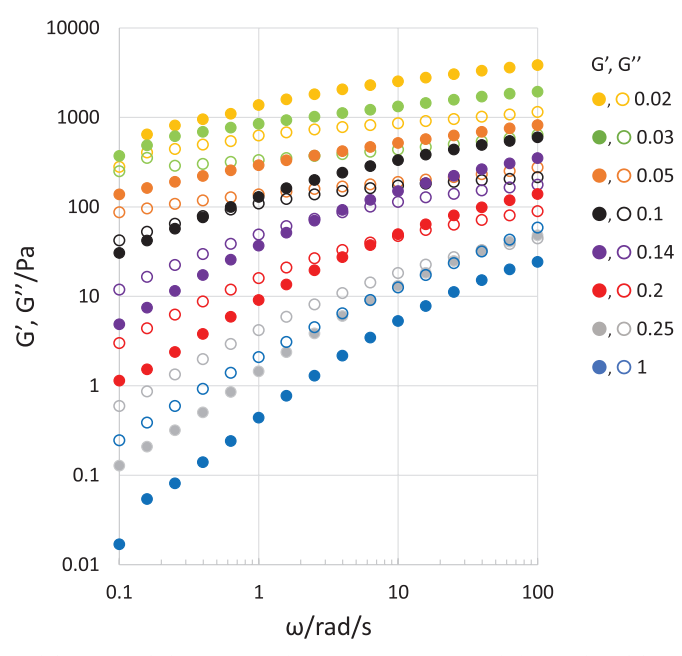


Fig. 6 Storage modulus (G') and loss modulus (G") of coacervate formed from the diluted shampoo at various relative concentrations as a function of frequency. The relative concentrations are indicated in the figure. Coacervate samples were prepared following the same procedure as described for the coacervate weight measurements in Fig. 2.

Figure 6 shows the storage modulus (G') and loss modulus (G'') from the same set of measurements. In the undiluted shampoo solution, G' < G'' over the entire measured frequency range, indicating that the viscous component dominates. However, for coacervates at relative concentrations between 0.1 and 0.25, G' and G'' intersect, with the intersection point shifting toward lower frequencies, implying longer relaxation times as the relative concentration decreases. For coacervates at relative concentrations below 0.05, G' > G'' across all measured frequencies, signifying the formation of a gel-like structure. Green and Tobolosky predicted that the high-frequency storage modulus is given by  $G_H = vkT$ , where v is the number density of elastically effective chains, v is the Boltzmann constant, and v is the absolute temperature.

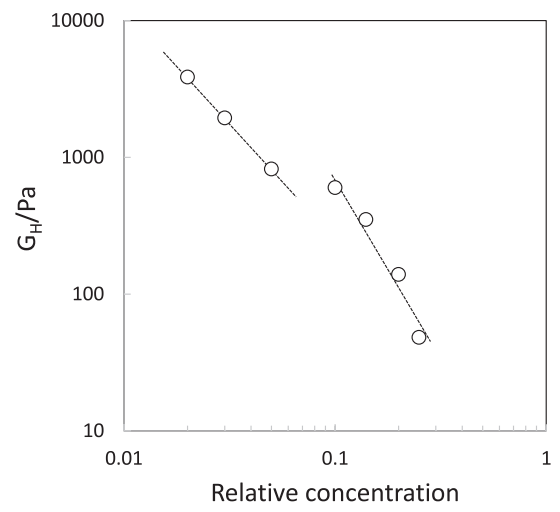


Fig. 7 High-frequency storage modulus  $(G_H)$  of the coacervate formed from diluted shampoo at various relative concentrations. The  $G_H$  values represent G' at 100 rad/s. Lines in the figure are included as visual guides.

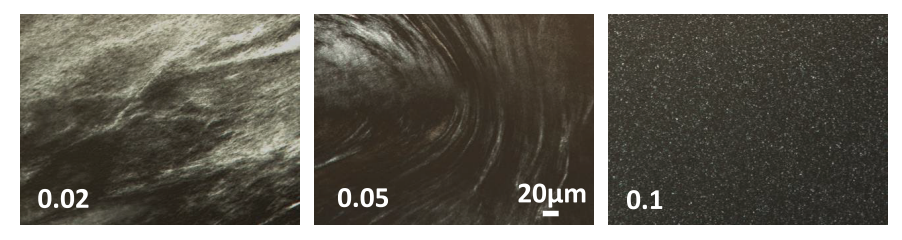


Fig. 8 Polarized light microscopic observation of the coacervate formed from diluted shampoo at relative concentrations of 0.02, 0.05, and 0.1. The coacervate samples were prepared following the same procedure used for coacervate amount measurements in Fig. 2. All the images shown were taken at the same magnification.

Figure 7 presents a plot of  $G_H$  values of the coacervate against relative concentrations. As the relative concentration decreases,  $G_H$  values increase, indicating that the density of the structural network contributing to elasticity becomes greater. This trend aligns with the observations reported by Ilekti et al.,<sup>33,34)</sup> where the solid concentration (polymer + surfactant) in the coacervate phase increases as counterions are released into the dilute phase during dilution. In Fig. 7, the relative concentration ranges from 0.1 to 0.25 and 0.02 to 0.05 plot as straight lines, respectively, while a gap is observed between the concentrations of 0.05 and 0.1, suggesting that a structural transition occurs within this concentration range.

# 3.6. Polarized light microscopy

Figure 8 presents polarized light microscope images of coacervates at relative concentrations of 0.02, 0.05, and 0.1. At a relative concentration of 0.1, microscopic dispersions exhibiting optical anisotropy were observed. In contrast, at concentrations of 0.05 and 0.02, textures characteristic of a lamellar phase, known as oily streaks, 50 became apparent. Additionally, structures with higher luminosity were more prominent at lower relative concentrations of coacervate.

#### 3.7. TEM

Figure 9 displays TEM images of the coacervate at a relative concentration of 0.05. The images represent the coacervate dispersion immediately after dilution, as the coacervate itself, with its high viscosity, as previously analyzed, was too thick to be thinned for the TEM observation. The TEM image also reveals that the dispersed coacervate particles are enveloped by a distinct multilayered structure.

# 3.8. **SAXS**

Figure 10 shows the SAXS results for coacervates at relative concentrations ranging from 0.02 to 0.3. At relative concentrations of 0.1 and 0.3, a single peak is observed at q values of 0.9 and 1.1 nm<sup>-1</sup>, respectively. However, at concentrations below 0.05, 2 distinct peaks appear in a 1:2 ratio, indicating the presence of a lamellar phase. The significant change in the SAXS profile between relative concentrations of 0.05 and 0.1 aligns with the structural transition observed in the viscoelasticity measurements and polarized microscopy observations, as previously described. Based on

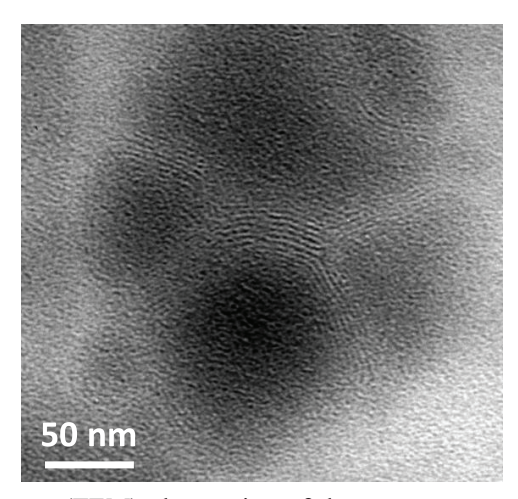


Fig. 9 Transmission electron microscopy (TEM) observation of the coacervate at a relative concentration of 0.05. The sample was analyzed immediately after dilution.

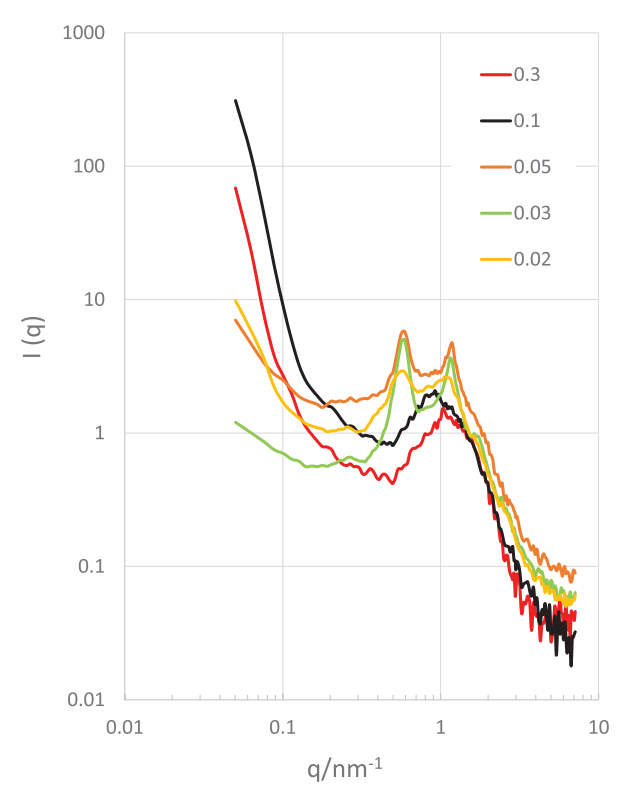


Fig. 10 Small-angle X-ray scattering (SAXS) profiles of coacervate formed from the diluted shampoo at various relative concentrations. The relative concentrations are indicated in the figure. Coacervate samples were prepared following the same procedure as described for the coacervate weight measurements in Fig. 2.

the results of polarized light microscopy, TEM observations, and SAXS measurements, it is suggested that the coacervate formed at a relative concentration of 0.05 or lower in the shampoo formulation examined here exhibits a lamellar structure.

Table 2 lists the lamellar interlayer distance (d-spacing/nm), calculated from the first peak position  $q_1$ , using the formula  $d = 2\pi/q_1$ . Interestingly, the lamellar interlayer distance remains constant, regardless of the relative concentration. From the GIFT (generalized indirect Fourier transformation) analysis results, <sup>51,52)</sup> it can be inferred that the lamellar layers overlap by 2–4 layers. These lamellar layers, consisting of surfactants, may be cross-linked by oppositely charged cationic polymers, forming a gel network in the coacervate. The network in the coacervate becomes denser with dilution, as implied by the rheology results.

Table 2 SAXS profile analysis of the coacervate formed from diluted shampoo at relative concentrations of 0.02–0.05. The d-spacing values were obtained using the equation  $d = 2\pi/q1$ .

Relative concentrations	$q_1$	$q_2$	d/nm
0.05	0.590	1.181	10.6
0.03	0.590	1.155	10.6
0.02	0.564	1.130	11.1

To elucidate the changes occurring during the shampoo dilution process, the experimental results obtained to date are summarized and discussed. As the shampoo is diluted with water, the system initially contains positively charged cationic polymers and negatively charged anionic/amphoteric surfactant mixed micelles. This state persists from the undiluted original shampoo solution up to a relative concentration of around 0.4, before coacervation occurs. Upon further dilution, once a critical relative concentration is surpassed, coacervation begins. This results in the formation of 2 distinct phases: (1) a coacervate phase, composed of a complex of hydrated polymers and mixed micelles, and (2) a dilute phase, consisting mostly of water, counterions, and excess surfactants.<sup>4,5,33,34)</sup> Initially, the coacervate does not have a well-defined structure, but with further dilution, the system undergoes more significant structural changes. As the relative concentration decreases and reaches around 0.05, the coacervate starts forming a lamellar structure.

The cationic polymers may connect the negatively charged lamellar layers by electrostatic forces, forming networks that result in an increase in the viscoelasticity of the coacervate observed in Figs. 5–7. However, the interlayer spacing of the lamellar structure remains constant, as shown in Table 2, suggesting that the polymer does not penetrate into the aqueous interlamellar layers but instead forms a network connecting the dispersed lamellar structures, which consist of 2–4 overlapping lamellar layers. As dilution continues, based on the fluorescence probe analysis shown in Fig. 4, starting around a relative concentration of 0.001, the system becomes too dilute to form enough micelles on the polymers. At relative concentrations below 0.00003, micelles are completely dissolved. At this stage, some anionic surfactants remain adsorbed onto the cationic polymers, while the majority of surfactants exist in a monomer state, no longer forming micelles.

In this study, we observed the coacervation phenomenon during the dilution process of a commercial non-sulfate shampoo, which is becoming increasingly popular in the market, and found many similarities with the coacervation behavior of LS/LES-based shampoos. However, few studies have reported coacervates adopting specific structures. Ilekti et al. previously reported that the NaPA /CTABr system forms a hexagonal structure.<sup>33,34</sup>) Reports of coacervates with lamellar structures are even rarer; to the best of our knowledge, only Seyrig et al.<sup>7</sup>) have documented a lamellar phase in a glycolipid/poly-L-lysine system at low pH.

Whether the formation of such lamellar phases is a characteristic feature of non-sulfate shampoo coacervates is currently under investigation using model shampoo formulations. We developed a model formulation system incorporating well-defined non-sulfate anionic surfactants and amphoteric surfactants of known composition alongside polymers of varying molecular weights and degrees of cationic modification at a variety of ionic strengths. This will allow us to investigate the influence of molecular weight, polymer charge density, counterion concentration, and surfactant composition ratios on coacervation behavior. These factors will be systematically studied, and the results will be reported separately.

# 4. Conclusion

The dilution of shampoo with water leads to electrostatic interactions between cationic polymers and anionic/amphoteric surfactants, the main components of shampoo, resulting in the formation of coacervates. In this study, we focused on a commercial non-sulfate shampoo and investigated the structural changes of the coacervate during the dilution process. As the shampoo was diluted, the coacervate became increasingly elastic, and at relative concentrations of 0.05 or lower, a lamellar structure emerged. With further dilution, the lamellar structure disappeared, and the coacervate eventually dissolved. To better understand these structural changes, which are commonly observed in non-sulfate shampoos, it will be essential to develop model formulation systems and continue investigating the effects of surfactant type and composition, polymer molecular weight, and the degree of cationic modification.

**Acknowledgments:** The authors thank Dr. Y. Takasaki and S. Otobe at Anton Paar Japan KK for their kind support with SAXS measurement and analysis. A part of this work was supported by the Advanced Research Infrastructure for Materials and Nanotechnology in Japan (ARIM) of the Ministry of Education, Culture, Sports, Science and Technology (MEXT) (Grant Number JPMXP1224UT).

#### Conflict of Interest: None.

**Abbreviations:** CAC, critical aggregation concentration; CTABr, cetyltrimethylammonium bromide; LS, lauryl sulfate; LES, sodium laureth sulfate; NaPA, sodium polyacrylate; P.I., polydispersity index; SAXS, small-angle X-ray scattering; TEM, transmission electron microscopy

## References

- 1) P.L. Dubin, M. Elayne, Y. Vea, M.A. Fallon, S.S. Thé, D.R. Rigsbee, L.M. Gan, Langmuir, 6, 1422–1427 (1990)
- 2) Y. Hiwatari, K. Yoshida, T. Akutsu, M. Yabu, S. Iwai, J. Soc. Cosmet. Chem. Jpn., 38, 211–219 (2004)
- 3) Y. Yamamoto, T. Ono, J. Soc. Cosmet. Chem. Jpn., 57, 50–57 (2023)
- 4) Y. Wang, K. Kimura, Q. Huang, P. L. Dubin, W. Jaeger, Macromolecules, 32, 7128–7134 (1999)
- 5) Y. Wang, K. Kimura, P. L. Dubin, W. Jaeger, Macromolecules, 33, 3324–3331 (2000)
- 6) E. Kizilay, A.B. Kayitmazer, P.L. Dubin, Adv. Colloid Interface Sci., 167, 24–37 (2011)
- 7) C. Seyrig, G. Kignelman, W. Thielemans, P.L. Griel, N. Cowieson, J. Perez, N. Baccile, Langmuir, 36, 8839–8857 (2020)
- 8) N. Kanei, T. Kodama, T. Harigai, J. Soc. Cosmet. Chem. Jpn., 51, 311–316 (2017)
- 9) E.D. Goddard, R.B. Hannan, J. Am. Oil Chem. Soc., 54, 561–566 (1977)
- 10) Q. Wang, J.B. Schlenoff, Macromolecules, 47, 3108–3116 (2014)
- 11) K. Ohbu, O. Hiraishi, I. Kashiwa, J. Am. Oil Chem. Soc., 59, 108–112 (1982)
- 12) K. Thalberg, B. Lindman, K. Bergfeld, Langmuir, 7, 2893–2898 (1991)
- 13) K. Thalberg, B. Lindman, G. Karlstrom, J. Phys. Chem., 94, 4289–4295 (1990)
- 14) K. Thalberg, B. Lindman, G. Karlstrom, J. Phys. Chem., 95, 3370–3376 (1991)
- 15) K. Thalberg, B. Lindman, G. Karlstrom, J. Phys. Chem., 95, 6004–6011 (1991)
- 16) M. Ghasemi, S.N. Jamadagni, E.S. Johnson, R.G. Larson, Langmuir, 39, 10335–10351 (2023)
- 17) C. Schmitt, S. L. Turgeon, Adv. Colloid Interface Sci., 167, 63–70 (2011)
- 18) B.D. Winslow, H. Shao, R.J. Stewart, P.A. Tresco, Biomaterials, 31, 9373–9381 (2010)
- 19) N.R. Johnson, Y. Wang, Expert Opin. Drug Deliv., 11, 1829–1832 (2014)
- 20) L. Chiappisi, M. Simon, M. Gradzielski, ACS Appl. Mater. Interfaces, 7, 6139–6145 (2015)
- 21) D.J. Burgess, S. Ponsart, J. Microencapsul., 15, 569–579 (1998)
- 22) Y. Wang, J. Gao, P.L. Dubin, Biotechnol. Prog., 12, 356–362 (1996)
- 23) O.G. Jones, U. Lesmes, P.L. Dubin, D.J. McClements, Food Hydrocoll., 24, 374–383 (2010)
- 24) K. Yoshida, Y. Morishima, P.L. Dubin, M. Mizusaki, Macromolecules, 30, 6208–6214 (1997)
- 25) K. Yoshida, S. Sokhakian, P. L. Dubin, J. Colloid Interface Sci., 205, 257–264 (1998)
- 26) P.L. Dubin, R. Oteri, J. Colloid Interface Sci., 95, 453–461 (1983)
- 27) P.L. Dubin, M.E. Curran, J. Hua, Langmuir, 6, 707–709 (1990)
- 28) D.W. McQuigg, J.I. Kaplan, P.L. Dubin, J. Phys. Chem., 96, 1973–1978 (1992)
- 29) L. Piculell, B. Lindman, Adv. Colloid Interface Sci., 41, 149–178 (1992)
- 30) M. Miyake, Adv. Colloid Interface Sci., 239, 146–157 (2017)
- 31) A.Y. Xu, E. Kizilay, S.P. Madro, J.Z. Vadenais, K.W. McDonald, P.L. Dubin, Soft Matter, 14, 2391–2399 (2018)
- 32) Y. Morishima, M. Mizusaki, K. Yoshida, P.L. Dubin, Colloids Surf. A Physicochem. Eng. Asp., 147, 149–159 (1999)
- 33) P. Ilekti, L. Piculell, F. Tournilhac, B. Cabane, J. Phys. Chem. B, 102, 344–351 (1998)
- 34) P. Ilekti, T. Martin, B. Cabane, L. Piculell, J. Phys. Chem. B, 103, 9831–9840 (1999)
- 35) M. Sakaguchi, E. Suenaga, K. Kawaguchi, J. Soc. Cosmet. Chem. Jpn., 53, 106-111 (2019)
- 36) M. Ezure, J. Jpn. Cosmet. Sci. Soc., 42, 15-20 (2018)
- 37) Y. Koizumi, Fragrance J., 50, 10–16 (2022)

- 38) Y. Yasuda, R. Tojo, Fragrance J., 49, 44–48 (2021)
- 39) H. Kamo, T. Mori, K. Yoshida, J. Soc. Cosmet. Chem. Jpn., Submitted for publication
- 40) E. Kizilay, A.B. Kayitmazer, P.L. Duin, Adv. Colloid Interface Sci., 167, 24-37 (2011)
- 41) M.E. Haque, S. Ray, A. Charkrabarti, J. Fluoresc., 10, 1-6 (2000)
- 42) D.C. Dong, M.A. Winnik, Photochem. Photobiol., 35, 17–21 (1982)
- 43) G.B. Ray, I. Chakraborty, S.P. Moulik, J. Colloid Interface Sci., 294, 248–254 (2006)
- 44) J. Gummel, F. Cousin, F. Boue, J. Am. Chem. Soc., 129, 5806–5807 (2007)
- 45) Z. Ou, M. Muthukumar, J. Chem. Phys., 124, 15492 (2006)
- 46) S. Park, R. Barnes, Y. Lin, B. Jeon, S. Najafi, K.T. Delaney, G.H. Fredrickson, J.E. Shea, D.S. Hwang, S. Han, Commun. Chem., 3, 83 (2020)
- 47) M. Ghasemi, S. Friedowitz, R.G. Larson, Soft Matter, 16, 10640–10656 (2020)
- 48) M.S. Green, A.V. Tobolsky, J. Chem. Phys., 14, 80-89 (1946)
- 49) T. Annable, R. Buscall, R. Ettelaie, D. Whittlestone, J. Rheol. (N.Y.N.Y.), 37, 695–726 (1993)
- 50) K. Aramaki, Oleoscience, 23, 37–41 (2023)
- 51) G. Fritz, A. Bergmann, O. Glatter, J. Chem. Phys., 113, 9733–9740 (2000)
- 52) B. Weyerich, J. Brunner-Popela, O. Glatter, J. Appl. Cryst., 32, 197–209 (1999)